Large-Angle Precession of Magnetization Maintained by a Microwave Voltage

Hiroshi Imamura[*] and Rie Matsumoto[†]

*National Institute of Advanced Industrial Science and Technology (AIST), Research Center for Emerging
Computing Technologies, Tsukuba, Ibaraki 305-8568, Japan*

Effects of a microwave voltage on magnetization precession are analyzed based on a macrospin model. The microwave voltage induces the oscillating anisotropy field through the voltage-controlled magnetic anisotropy (VCMA) effect, and then stimulates the magnetization. The large-angle precession is maintained if the magnetization synchronizes with the microwave voltage. The effective equations of motion of the magnetization with an oscillating anisotropy field are derived, and the mechanism of the synchronization is clarified by analyzing the derived equations of motion. The conditions of the angular frequency detuning and the amplitude of the oscillating anisotropy field for synchronization are obtained. The results are useful for development of VCMA-based energy-efficient spintronic devices using magnetization precession such as a VCMA-based magnetoresistive random-access memory and a nanoscale microwave magnetic field generator.

I. INTRODUCTION

Magnetic anisotropy (MA) is a key property of a ferromagnet, which stabilizes the direction of magnetization even at room temperature [1,2]. In a magnetoresistive random-access memory (MRAM) the information is stored as the direction of magnetization, e.g., up or down. The height of the energy barrier between the up and down states is proportional to the MA constant, and the retention time of the information is an exponential increasing function of the MA constant [3]. The current standard writing scheme of MRAM utilizes the spin-transfer torque (STT) [4–6] because of low-power consumption and high integration density compared with the magnetic field switching. The STT acts as the negative damping torque and excites the magnetization over the energy barrier.

Discovery of the voltage-controlled magnetic anisotropy (VCMA) effect [7–13] provided a more energy-efficient writing scheme of MRAM. In VCMA-based switching [14–24], application of the voltage to the MRAM cell eliminates the MA of the free layer (FL) and induces the precession of magnetization around the external magnetic field. The switching completes if the voltage is turned off at a half period of precession. The power consumption of VCMA-based switching is much smaller than that of STT-based switching because of little Joule heating [16,17].

Parametric excitation (PE) is a nonlinear phenomenon induced by periodic modulation of a parameter in equations of motion and, which has been studied in many areas of physics and engineering [25]. In magnetic materials PE of magnetization is induced by applying a microwave field [26–36], microwave current [37–39], or microwave voltage [40–44]. The PE of the spin waves by microwave voltage in ferromagnetic films [40–42] attracts much attention as a key element of low-power consumption magnonic devices [45].

Recently, Yamamoto *et al.* [44] studied the effect of PE on VCMA-based switching in a MRAM cell and found that the oscillation amplitude of the switching probability does not decay if the magnetization precesses in synchronization with the applied oscillating voltage. They also performed the numerical simulations based on the macrospin model and reproduced the experimental results very well. Although the results are qualitatively and intuitively explained by the concept of PE, more detailed theoretical analysis on the mechanism as well as the conditions for PE in this system is necessary for practical applications. Since the experimental situation is quite different from PE of spin waves in ferromagnetic films, the theory developed by Verba *et al.* [40–42] is not directly applicable for the analysis of the results in Ref. [44].

In this paper, we analyze the effects of a microwave voltage on magnetization precession using the macrospin model following the standard analysis of PE [25]. It is shown that the large-angle precession is maintained if the magnetization synchronizes with the microwave voltage. The mechanism of the synchronization is clarified, and the conditions of parameters for synchronization are

_____

[*]h-imamura@aist.go.jp
[†]rie-matsumoto@aist.go.jp

obtained by analyzing the effective equations of motion of the magnetization under the microwave voltage.

The results are useful for reducing the write error rate of VCMA-based MRAM by using a microwave voltage pulse. The large-angle precession of magnetization maintained by a microwave voltage can be applied as a low-power nanoscale microwave magnetic field generator.

II. MODEL AND METHOD

The system we consider is schematically shown in Fig. 1(a). The FL of a VCMA-based MRAM with perpendicular MA is shown in gray. Application of a voltage, V, modifies the electron state at the interface between the FL and insulating layer shown in black and changes the MA of the FL through the VCMA effect. The white cylinders represent the other layers, such as the reference layer and electrodes. The definition of the coordinate system is shown in Fig. 1(b). In terms of the polar angle θ and the azimuthal angle ϕ, the magnetization unit vector $\mathbf{m}$ is expressed as $\mathbf{m} = (m_x, m_y, m_z) = (\sin\theta\cos\phi, \sin\theta\sin\phi, \cos\theta)$. The external magnetic field H_{ext} is applied in the positive z direction and the perpendicular anisotropy field is parallel to the x axis. The voltage is assumed to be the sum of the static and oscillating components, expressed as $V = V_{\text{st}} + V_{\text{osc}}$. The static component V_{st} is assumed to be large enough to eliminate the static MA of the FL. The oscillating component V_{osc} generates the oscillating anisotropy field and stimulates the magnetization.

In order to simplify the notation, the dimensionless forms of the magnetic field and time are introduced. The external field H_{ext} is taken as the unit of the magnetic field.
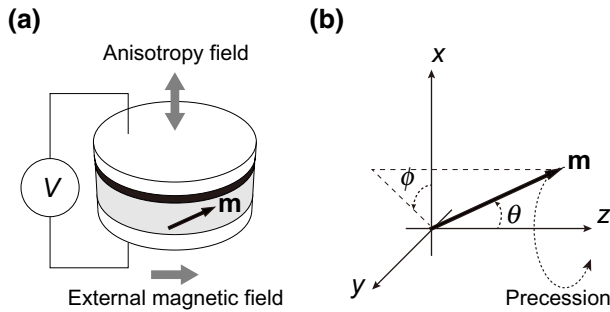
(a)

(b)

FIG. 1. (a) Schematic illustration of the FL in the VCMA-based MRAM. The FL shown in gray is a thin magnetic layer with a perpendicular MA. Here $\mathbf{m}$ represents the magnetization unit vector. The insulating layer is shown in black. The other layers, such as the reference layer and electrodes, are shown in white. The external magnetic field is applied to the in-plane direction. The anisotropy field is modified by application of a voltage, V. (b) Definitions of the Cartesian coordinates, and the polar angle θ and azimuthal angle ϕ of $\mathbf{m}$. The perpendicular anisotropy field is parallel to the x axis. The external field is applied in the positive z direction. The direction of magnetization precession is indicated by the dotted circular arrow.

The unit of time is set as $(1 + \alpha^2)/(\gamma H_{\text{ext}})$, where α is the Gilbert damping constant and γ is the gyromagnetic ratio.

The oscillating anisotropy field induced by V_{osc} is given by

$$h_k \cos(\omega\tau)\sin\theta\cos\phi, \qquad (1)$$

where h_k is the amplitude of the oscillating anisotropy field, and ω and τ are the angular frequency of V_{osc} and time in the dimensionless unit, respectively. The dynamics of $\mathbf{m}$ is obtained by solving the Landau-Lifshitz-Gilbert (LLG) equation

$$\dot{\theta} = -\alpha\sin\theta - h_k\cos(\omega\tau)\sin\theta\cos\phi$$
$$\times (\sin\phi - \alpha\cos\theta\cos\phi), \qquad (2)$$

$$\dot{\phi} = 1 - h_k\cos(\omega\tau)\cos\phi(\cos\theta\cos\phi + \alpha\sin\theta), \quad (3)$$

where the dot represents the derivative in terms of τ. The values of α and h_k are assumed to be much smaller than unity. For numerical simulations and exemplification of the analytical results, we assume that $\alpha = 0.01$ and $h_k = 0.05$ unless otherwise mentioned. In numerical simulations the fourth-order Runge-Kutta method is employed to solve the LLG equation. Before application of the voltage, the magnetization is aligned perpendicular to the plane because the FL has a static perpendicular MA. The initial state is assumed to be $m_x = 1$, i.e., $\theta = \pi/2$ and $\phi = 0$.

III. RESULTS AND DISCUSSIONS

In Fig. 2(a) we present a color density plot of m_x in the τ-ω plane, which can be observed owing to the magnetoresistance effect. The large amplitude of oscillation is maintained around twice the natural angular frequency of precession, i.e., $\omega = 2$. In Ref. [44], similar plots were obtained for the switching probabilities. An enlarged view for $1.8 \leq \omega \leq 2.2$ is shown in Fig. 2(b). The region of angular frequency where the large amplitude of oscillation is maintained is $1.98 \lesssim \omega \lesssim 2.02$. Outside of this synchronization region the oscillation amplitude shows a monotonic decay.

The dynamics of m_x and m_z at $\omega = 1$ is plotted in Fig. 2(c). We see that m_z increases with increasing τ, approaching unity, and that m_x shows damped oscillation with a period of 2π. These results agree well with the exact solutions for $h_k = 0$ [2], which implies that V_{osc} with $\omega = 1$ has little effect on the magnetization dynamics.

The same plot at $\omega = 2$ is shown in Fig. 2(d). Contrary to the results at $\omega = 1$, the oscillation amplitude does not show monotonic decay. Although the oscillation amplitude decays for $\tau \lesssim 100$, it takes the minimum value at $\tau \approx 100$ and then increases with increasing τ. The period
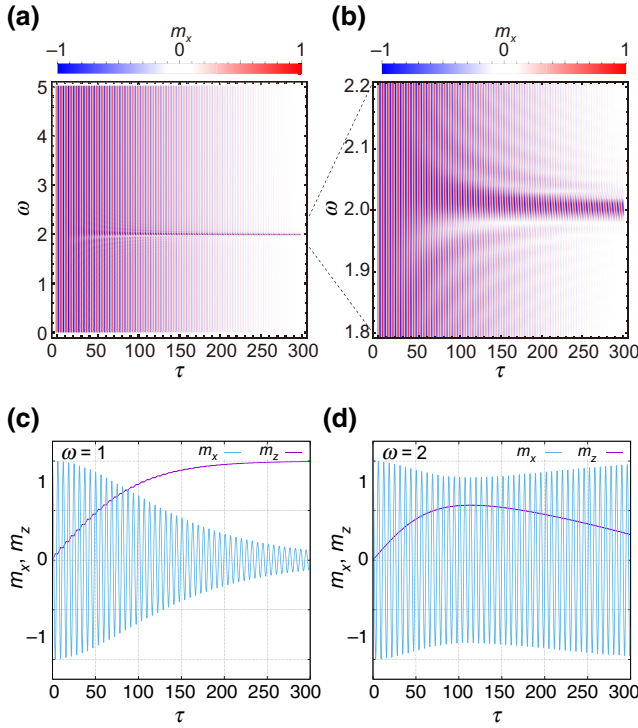
(a)

(b)

(c)

(d)

FIG. 2. (a) A color density plot of m_x in the ω-τ plane. Around $\omega = 2$ the large-angle precession of magnetization is maintained by the microwave voltage. (b) An enlarged view of panel (a) for $1.8 \leq \omega \leq 2.2$. The synchronization region is about $1.98 \lesssim \omega \lesssim 2.02$ at $\tau = 300$. (c) The dynamics of m_x and m_z for the non-synchronized state at $\omega = 1$. The precession amplitude decays monotonically. (d) The same plot as (c) for the synchronized state at $\omega = 2$. The precession amplitude increases with increasing τ in the region $\tau \gtrsim 100$.

of oscillation is 2π, i.e., **m** oscillates with the natural angular frequency of unity instead of the angular frequency of V_{osc}, $\omega = 2$. The fact that the precession amplitude of **m** is strongly enhanced by the external periodic force with twice the natural angular frequency implies that this phenomena is closely related to parametric excitation [26–28, 30–33,38,43].

In Fig. 3(a) we show the dynamics of the polar angle θ at $\omega = 2$ for a long time duration of $\tau \leq 20\,000$. In Fig. 3(b) we present the same plot for the phase shift from the free precession at an angular frequency of $\omega/2$, which is defined as

$$\Delta\phi = \phi - \frac{\omega}{2}\tau. \quad (4)$$

The polar angle is a measure of the oscillation amplitude because $m_x = \sin\theta$. The azimuthal angle ϕ represents the oscillation phase, and the phase shift $\Delta\phi$ is closely related to the energy absorption. The polar angle shows a slow oscillation with a period much longer than 2π and converges to about $\pi/2$ for large τ. The phase shift also shows
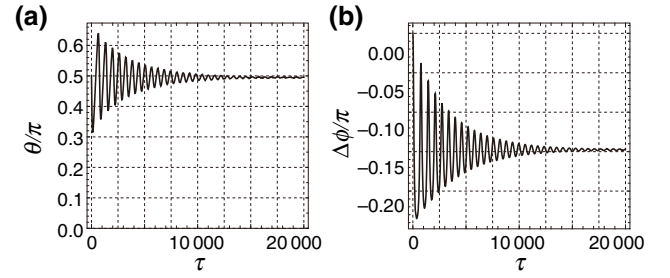
(a)

(b)

FIG. 3. (a) The dynamics θ at $\omega = 2$ for $0 \leq \tau \leq 20\,000$. It oscillates with a period much longer than 2π and converges to about $\pi/2$ for large τ. (b) The same plot as (a) for $\Delta\phi$. It oscillates with the same period as θ and converges to about -0.148π for large τ.

the slow oscillation with the same period as the polar angle and converges to about -0.148π for large τ.

The equation of motion for the slow dynamics of the polar angle is derived as follows. Since both α and h_k are assumed to be much smaller than unity, the terms with αh_k can be neglected in the LLG equation. Then Eq. (2) becomes

$$\dot{\theta} = -\alpha \sin\theta - h_k \cos(\omega\tau) \sin\theta \cos\phi \sin\phi. \quad (5)$$

The second term on the right-hand side depends on ϕ as $\cos\phi\sin\phi$, where $\cos\phi$ comes from m_x, and $\sin\phi$ is the projection coefficient of the anisotropy field torque to the direction of $\dot{\theta}$. Since $\cos\phi\sin\phi = \sin(2\phi)/2$, ω should be twice the angular frequency of magnetization precession to realize synchronization.

Substituting $\phi = \omega\tau/2 + \Delta\phi$ into Eq. (5) and applying the trigonometric identities we obtain

$$\dot{\theta} = -\sin\theta\left\{\alpha + \frac{h_k}{4}[\sin(2\Delta\phi) + \sin(2\omega\tau + 2\Delta\phi)]\right\}. \quad (6)$$

Since we are interested in the slow dynamics of θ and $\Delta\phi$, we average out the fast oscillating term with $\sin(2\omega\tau + 2\Delta\phi)$. Finally, the equation of motion for the slow dynamics of θ is obtained as

$$\dot{\theta} = -\sin\theta\left[\alpha + \frac{h_k}{4}\sin(2\Delta\phi)\right]. \quad (7)$$

Introducing the effective damping coefficient defined as

$$\alpha' = \alpha + \frac{h_k}{4}\sin(2\Delta\phi), \quad (8)$$

Eq. (7) is expressed as $\dot{\theta} = -\alpha' \sin\theta$, which is the same form as Eq. (2) with $h_k = 0$. Assuming that $\dot{\theta} = 0$ and $\sin\theta \neq 0$ in the limit of $\tau \to \infty$, the convergence value of the phase shift, $\Delta\phi_c$, should be adjusted to satisfy

$\sin(2\Delta\phi_c) = -4\alpha/h_k$. There are two kinds of solutions for this equation:

$$\Delta\phi_c^{(-)} = -\frac{1}{2}\arcsin\left(\frac{4\alpha}{h_k}\right) \qquad (9)$$

and

$$\Delta\phi_c^{(+)} = -\frac{\pi}{2} + \frac{1}{2}\arcsin\left(\frac{4\alpha}{h_k}\right). \qquad (10)$$

For the parameters we assumed, i.e., $\alpha = 0.01$ and $h_k = 0.05$, $\Delta\phi_c^{(-)} = -0.148\pi$, which is identical to the numerical result shown in Fig. 3(b).

The equation of motion for the slow dynamics of $\Delta\phi$ is obtained in a similar manner. Substituting $\phi = \omega\tau/2 + \Delta\phi$ into Eq. (3), neglecting the term with αh_k, and averaging out the fast oscillating term, we obtain

$$\dot{\Delta\phi} = 1 - \frac{\omega}{2} - \frac{h_k}{4}\cos\theta\cos(2\Delta\phi). \qquad (11)$$

Equation (11) is reduced to $\dot{\Delta\phi} = -(h_k/4)\cos\theta\cos(2\Delta\phi)$ at $\omega = 2$. Assuming that $\cos(2\Delta\phi) > 0$, i.e., $|\Delta\phi| < \pi/2$, the sign of $\dot{\Delta\phi}$ is determined by the sign of $\cos\theta$. The phase shift $\Delta\phi$ increases (decreases) with increasing τ if $\theta > \pi/2$ ($\theta < \pi/2$).

To understand the mechanism of synchronization, we analyze the dynamics of θ, $\Delta\phi$, and α' in the first two and a half periods of oscillation. In Fig. 4 we show the dynamics of θ (top), $\Delta\phi$ (middle), and α' (bottom) at $\omega = 2$ for $0 \leq \tau \leq 2000$. The horizontal dashed lines in the top, middle, and bottom panels represent the values $\frac{1}{2}$, $\Delta\phi_c^{(-)}/\pi$, and 0, respectively. The vertical dotted lines represent the values of τ at which $\Delta\phi$ takes the convergence value of $\Delta\phi_c^{(-)}$.

At the beginning of the dynamics, θ decreases with increasing τ because $\alpha' \simeq \alpha$ (> 0). The phase shift $\Delta\phi$ also decreases with increasing τ because $\theta < \pi/2$. The decrease in $\Delta\phi$ induces a reduction in α' following Eq. (8). When $\Delta\phi$ crosses the horizontal dashed line, i.e., $\Delta\phi = \Delta\phi_c^{(-)}$, θ takes the minimum value and then starts to increase with increasing τ because α' becomes negative. However, $\Delta\phi$ and α' decrease with increasing τ until θ exceeds $\pi/2$. At $\tau \approx 400$, θ crosses the horizontal dashed line at $\theta = \pi/2$. Then both $\Delta\phi$ and α' take the minimum values and start to increase with increasing τ. Repeating the above procedure, θ, $\Delta\phi$, and α oscillate with the same period as each other and converge to the values $\pi/2$, $\Delta\phi_c^{(-)}$, and 0, respectively.

Let us move on to the analysis of the effect of angular frequency detuning on synchronization. The angular frequency detuning is defined as the difference between the angular frequency of V_{osc} and twice the natural angular frequency of the magnetization precession, i.e., $\nu = \omega - 2$.
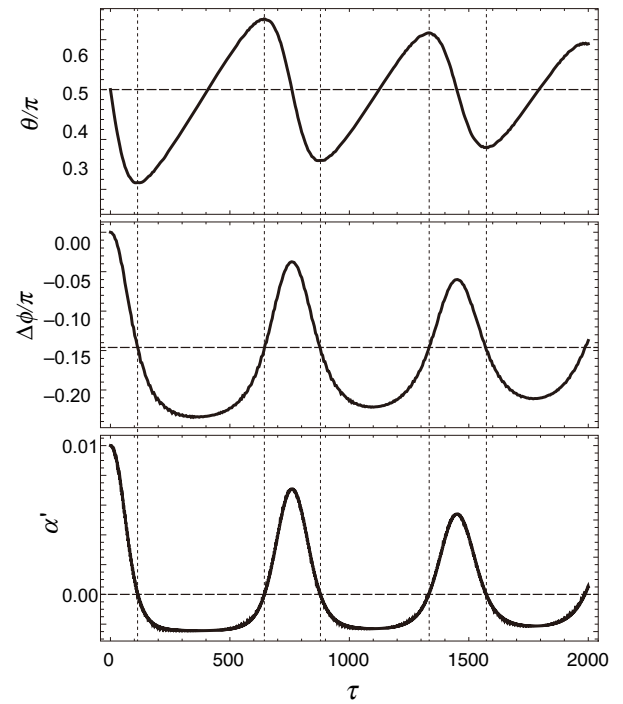

FIG. 4.   The dynamics of θ (top), $\Delta\phi$ (middle), and α' (bottom) at $\omega = 2$ for $0 \leq \tau \leq 2000$. The horizontal dashed lines in the top, middle, and bottom panels represent the values $\frac{1}{2}$, $\Delta\phi_c^{(-)}/\pi$, and 0, respectively. The vertical dotted lines represent the values of τ at which $\Delta\phi$ takes the convergence value of $\Delta\phi_c^{(-)}$.

As shown in Fig. 2(b), **m** synchronizes with V_{osc} within the range $-0.02 \lesssim \nu \lesssim 0.02$ at $\tau = 300$. The synchronization region of ν in the limit $\tau \to \infty$ is obtained as follows. Substituting $\omega = 2 + \nu$ into Eq. (11) we obtain

$$\dot{\Delta\phi} = -\frac{\nu}{2} - \frac{h_k}{4}\cos\theta\cos(2\Delta\phi). \qquad (12)$$

Assuming that $\lim_{\tau\to\infty}\dot{\Delta\phi} = 0$ and $\lim_{\tau\to\infty}\Delta\phi = \Delta\phi_c^{(-)}$, the convergence value of θ is obtained by solving

$$-\frac{\nu}{2} - \frac{h_k}{4}\cos\theta_c\cos(2\Delta\phi_c^{(-)}) = 0 \qquad (13)$$

as

$$\theta_c^{(-)} = \arccos\left[-\frac{2\nu}{\sqrt{h_k^2 - 16\alpha^2}}\right], \qquad (14)$$

which is valid for $\nu \leq 0$ because the convergence value of θ should satisfy $0 \leq \theta_c^{(-)} \leq \pi/2$.

The convergence value of θ for the case with $\lim_{\tau\to\infty}\Delta\phi = \Delta\phi_c^{(+)}$ is obtained in a similar manner as

$$\theta_c^{(+)} = \arccos\left[\frac{2\nu}{\sqrt{h_k^2 - 16\alpha^2}}\right], \qquad (15)$$

which is valid for $\nu \geq 0$. At $\nu = 0$, $\theta_c = \pi/2$ and both $\Delta\phi_c^{(-)}$ and $\Delta\phi_c^{(+)}$ are the valid solutions. Since $\Delta\phi_c^{(-)} \neq \Delta\phi_c^{(+)}$, it might be difficult to achieve a stable oscillation.

The general expressions of the convergence values of θ and $\Delta\phi$ are summarized as

$$\Delta\phi_c = -\frac{\pi(\nu + |\nu|)}{4} + \frac{\nu}{|\nu|}\frac{1}{2}\arcsin\left(\frac{4\alpha}{h_k}\right), \quad (16)$$

$$\theta_c = \arccos\left[\frac{2|\nu|}{\sqrt{h_k^2 - 16\alpha^2}}\right]. \quad (17)$$

The synchronization region of ν is obtained by requiring $\theta_c > 0$ as

$$|\nu| < \frac{1}{2}\sqrt{h_k - 16\alpha^2}. \quad (18)$$

The synchronization condition of h_k is obtained in a similar manner as

$$h_k > 2\sqrt{\nu^2 + 4\alpha^2}. \quad (19)$$

In the limit $\nu \to 0$, the critical value of h_k is obtained as 4α.

In Fig. 5(a) we show the ν dependence of θ_c. The analytical results of Eq. (17) are shown in the top panel. The numerical results obtained by solving Eqs. (2) and (3) for $\tau \leq 20\,000$ are shown in the bottom panel. Although the analytical results are almost identical to the numerical results, the small sharp peak appears in the vicinity of $\nu = 0$ in the numerical results. At this value of ν, the numerical simulations do not converge even at $\tau = 20\,000$.

In Fig. 5(b) we present color density plots of the phase shift in the synchronization region in the ν-h_k plane. The analytical results of Eqs. (16) and (19) are shown in the top panel. The numerical results obtained by solving Eqs. (2) and (3) for $\tau \leq 20\,000$ are shown in the bottom panel, where the synchronization region is defined to satisfy $\theta > 0.01$ at $\tau = 20\,000$. In both panels the red and blue tones represent $\Delta\phi_c^{(-)}$ and $\Delta\phi_c^{(+)}$, respectively. The analytical results are almost identical to the numerical results. However, the boundary between $\Delta\phi_c^{(-)}$ and $\Delta\phi_c^{(+)}$ in the numerical results shifts slightly toward larger ν from the analytical boundary at $\nu = 0$. This small deviation is caused by the terms with αh_k that we neglect in the analytical calculations.

IV. SUMMARY

In summary, the effects of microwave voltage on the magnetization dynamics in the FL of a VCMA-based MRAM is theoretically analyzed. It is shown that the large-angle precession of magnetization is maintained if the angular frequency of the microwave voltage is about
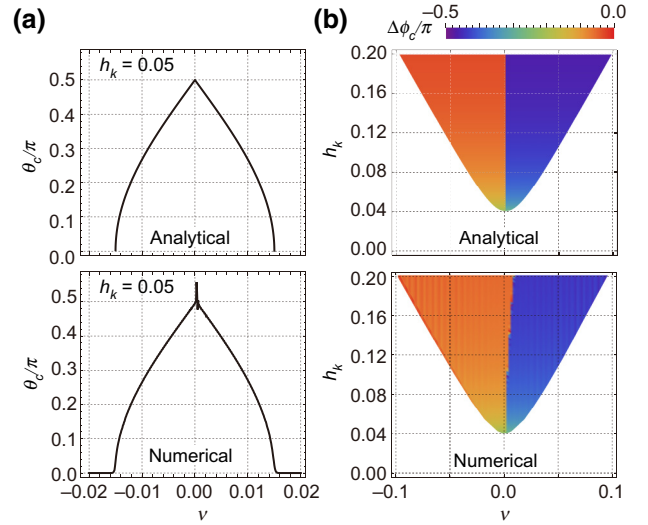

FIG. 5. (a) The ν dependence of θ_c obtained by analytical calculation (top) and numerical simulation at $\tau = 20\,000$ (bottom). (b) Color density plots of $\Delta\phi_c$ obtained by analytical calculation (top) and numerical simulation at $\tau = 20\,000$ (bottom) in the ν-h_k plane.

twice the natural angular frequency of the precession. The effective equations of motion for the slow dynamics of the polar angle and the phase shift are derived. The mechanism of the synchronization is explained by analyzing the slow dynamics of the polar angle, phase shift, and effective damping coefficient. The phase shift is automatically adjusted to eliminate the effective damping. The convergence value of the phase shift strongly depends on the sign of the angular frequency detuning. The synchronization conditions of the angular frequency detuning and the amplitude of the oscillating anisotropy field are obtained. The critical value of the amplitude of the oscillating anisotropy field is proportional to the Gilbert damping constant. The results are useful for development of VCMA-based energy-efficient spintronic devices using magnetization precession such as a VCMA-based MRAM and a nanoscale microwave magnetic field generator.

[1] S. Chikazumi, *Physics of Ferromagnetism* (Oxford : Clarendon press, New York, 1997).

[2] L. D. Landau and E. M. Lifshits, *Electrodynamics of Continuous Media* (Pergamon Press, Oxford; New York, 1960).

[3] W. F. Brown, Thermal fluctuations of a single-domain particle, Phys. Rev. **130**, 1677 (1963).

[4] J. C. Slonczewski, Current-driven excitation of magnetic multilayers, J. Magn. Magn. Mater. **159**, L1 (1996).

[5] L. Berger, Emission of spin waves by a magnetic multilayer traversed by a current, Phys. Rev. B **54**, 9353 (1996).

[6] M. D. Stiles and J. Miltat, in *Topics in Applied Physics* (Springer Berlin Heidelberg, 2006) , Vol. 101 p. 225.

[7] M. Weisheit, S. Fahler, A. Marty, Y. Souche, C. Poinsignon, and D. Givord, Electric field-induced modification of magnetism in thin-film ferromagnets, Science **315**, 349 (2007).

[8] C.-G. Duan, J. P. Velev, R. F. Sabirianov, Z. Zhu, J. Chu, S. S. Jaswal, and E. Y. Tsymbal, Surface Magnetoelectric Effect in Ferromagnetic Metal Films, Phys. Rev. Lett. **101**, 137201 (2008).

[9] M. Tsujikawa and T. Oda, Finite Electric Field Effects in the Large Perpendicular Magnetic Anisotropy Surface Pt/Fe/Pt(001): A First-Principles Study, Phys. Rev. Lett. **102**, 247203 (2009).

[10] K. Nakamura, R. Shimabukuro, Y. Fujiwara, T. Akiyama, T. Ito, and A. J. Freeman, Giant Modification of the Magnetocrystalline Anisotropy in Transition-Metal Monolayers by an External Electric Field, Phys. Rev. Lett. **102**, 187201 (2009).

[11] T. Maruyama, Y. Shiota, T. Nozaki, K. Ohta, N. Toda, M. Mizuguchi, A. A. Tulapurkar, T. Shinjo, M. Shiraishi, S. Mizukami, Y. Ando, and Y. Suzuki, Large voltage-induced magnetic anisotropy change in a few atomic layers of iron, Nat. Nanotechnol. **4**, 158 (2009).

[12] T. Nozaki, Y. Shiota, M. Shiraishi, T. Shinjo, and Y. Suzuki, Voltage-induced perpendicular magnetic anisotropy change in magnetic tunnel junctions, Appl. Phys. Lett. **96**, 3 (2010).

[13] M. Endo, S. Kanai, S. Ikeda, F. Matsukura, and H. Ohno, Electric-field effects on thickness dependent magnetic anisotropy of sputtered MgO/Co40Fe40B20/Ta structures, Appl. Phys. Lett. **96**, 3 (2010).

[14] Y. Shiota, T. Nozaki, F. Bonell, S. Murakami, T. Shinjo, and Y. Suzuki, Induction of coherent magnetization switching in a few atomic layers of FeCo using voltage pulses, Nat. Mater. **11**, 39 (2012).

[15] S. Kanai, M. Yamanouchi, S. Ikeda, Y. Nakatani, F. Matsukura, and H. Ohno, Electric field-induced magnetization reversal in a perpendicular-anisotropy CoFeB-MgO magnetic tunnel junction, Appl. Phys. Lett. **101**, 122403 (2012).

[16] C. Grezes, F. Ebrahimi, J. G. Alzate, X. Cai, J. A. Katine, J. Langer, B. Ocker, P. Khalili Amiri, and K. L. Wang, Ultra-low switching energy and scaling in electric-field-controlled nanoscale magnetic tunnel junctions with high resistance-area product, Appl. Phys. Lett. **108**, 3 (2016).

[17] S. Kanai, F. Matsukura, and H. Ohno, Electric-field-induced magnetization switching in CoFeB/MgO magnetic tunnel junctions with high junction resistance, Appl. Phys. Lett. **108**, 192406 (2016).

[18] R. Matsumoto, T. Nozaki, S. Yuasa, and H. Imamura, Voltage-Induced Precessional Switching at Zero-Bias Magnetic Field in a Conically Magnetized Free Layer, Phys. Rev. Appl. **9**, 014026 (2018).

[19] T. Yamamoto, T. Nozaki, Y. Shiota, H. Imamura, S. Tamaru, K. Yakushiji, H. Kubota, A. Fukushima, Y. Suzuki, and S. Yuasa, Thermally Induced Precession-Orbit Transition of Magnetization in Voltage-Driven Magnetization Switching, Phys. Rev. Appl. **10**, 024004 (2018).

[20] H. Imamura and R. Matsumoto, Impact of Spin-Transfer Torque on the Write-Error Rate of a Voltage-Torque-Based Magnetoresistive Random-Access Memory, Phys. Rev. Appl. **11**, 064019 (2019).

[21] R. Matsumoto, T. Sato, and H. Imamura, Voltage-induced switching with long tolerance of voltage-pulse duration in a perpendicularly magnetized free layer, Appl. Phys. Express **12**, 053003 (2019).

[22] T. Yamamoto, T. Nozaki, H. Imamura, Y. Shiota, T. Ikeura, S. Tamaru, K. Yakushiji, H. Kubota, A. Fukushima, Y. Suzuki, and S. Yuasa, Write-Error Reduction of Voltage-Torque-Driven Magnetization Switching by a Controlled Voltage Pulse, Phys. Rev. Appl. **11**, 014013 (2019).

[23] T. Yamamoto, T. Nozaki, H. Imamura, S. Tamaru, K. Yakushiji, H. Kubota, A. Fukushima, Y. Suzuki, and S. Yuasa, Voltage-Driven Magnetization Switching Using Inverse-Bias Schemes, Phys. Rev. Appl. **13**, 014045 (2020).

[24] R. Matsumoto and H. Imamura, Low-Power Switching of Magnetization Using Enhanced Magnetic Anisotropy with Application of a Short Voltage Pulse, Phys. Rev. Appl. **14**, 021003 (2020).

[25] A. H. Nayfeh and D. T. Mook, in *Nonlinear Oscillations* (John Wiley & Sons, Ltd, 2007), Chap. 5, p. 258.

[26] N. Bloembergen and R. W. Damon, Relaxation effects in ferromagnetic resonance, Phys. Rev. **85**, 699 (1952).

[27] N. Bloembergen and S. Wang, Relaxation effects in para - and ferromagnetic resonance, Phys. Rev. **93**, 72 (1954).

[28] P. W. Anderson and H. Suhl, Instability in the motion of ferromagnets at high microwave power levels, Phys. Rev. **100**, 1788 (1955).

[29] S. Urazhdin, P. Tabor, V. Tiberkevich, and A. Slavin, Fractional Synchronization of Spin-Torque Nano-Oscillators, Phys. Rev. Lett. **105**, 104101 (2010).

[30] S. Urazhdin, V. Tiberkevich, and A. Slavin, Parametric Excitation of a Magnetic Nanocontact by a Microwave Field, Phys. Rev. Lett. **105**, 237204 (2010).

[31] H. Ulrichs, V. E. Demidov, S. O. Demokritov, and S. Urazhdin, Parametric excitation of eigenmodes in microscopic magnetic dots, Phys. Rev. B **84**, 094401 (2011).

[32] S. Y. Martin, N. de Mestier, C. Thirion, C. Hoarau, Y. Conraux, C. Baraduc, and B. Diény, Parametric oscillator based on nonlinear vortex dynamics in low-resistance magnetic tunnel junctions, Phys. Rev. B **84**, 144434 (2011).

[33] E. R. J. Edwards, H. Ulrichs, V. E. Demidov, S. O. Demokritov, and S. Urazhdin, Parametric excitation of magnetization oscillations controlled by pure spin current, Phys. Rev. B **86**, 134420 (2012).

[34] J.-G. Zhu, X. Zhu, and Y. Tang, Microwave assisted magnetic recording, IEEE Trans. Magn. **44**, 125 (2008).

[35] L. Lu, M. Wu, M. Mallary, G. Bertero, K. Srinivasan, R. Acharya, H. Schultheiß, and A. Hoffmann, Observation of microwave-assisted magnetization reversal in perpendicular recording media, Appl. Phys. Lett. **103**, 2 (2013).

[36] W. Zhou, T. Yamaji, T. Seki, H. Imamura, and K. Takanashi, Resonant magnetization switching conditions of an exchange-coupled bilayer under spin wave excitation, Appl. Phys. Lett. **110**, 082401 (2017).

[37] Y.-T. Cui, J. C. Sankey, C. Wang, K. V. Thadani, Z.-P. Li, R. A. Buhrman, and D. C. Ralph, Resonant spin-transfer-driven switching of magnetic devices assisted by microwave current pulses, Phys. Rev B **77**, 214440 (2008).

[38] P. Dürrenfeld, E. Iacocca, J. Åkerman, and P. K. Muduli, Parametric excitation in a magnetic tunnel junction-based spin torque oscillator, Appl. Phys. Lett. **104**, 052410 (2014).

[39] E. A. Montoya, S. Perna, Y.-J. Chen, J. A. Katine, M. D'Aquino, C. Serpico, and I. N. Krivorotov, Magnetization reversal driven by low dimensional chaos in a nanoscale ferromagnet, Nat. Commun. **10**, 543 (2019).

[40] R. Verba, V. Tiberkevich, I. Krivorotov, and A. Slavin, Parametric Excitation of Spin Waves by Voltage-Controlled Magnetic Anisotropy, Phys. Rev. Appl. **1**, 044006 (2014).

[41] R. Verba, M. Carpentieri, G. Finocchio, V. Tiberkevich, and A. Slavin, Excitation of propagating spin waves in ferromagnetic nanowires by microwave voltage-controlled magnetic anisotropy, Sci. Rep. **6**, 25018 (2016).

[42] R. Verba, M. Carpentieri, G. Finocchio, V. Tiberkevich, and A. Slavin, Excitation of Spin Waves in an In-Plane-Magnetized Ferromagnetic Nanowire Using Voltage-Controlled Magnetic Anisotropy, Phys. Rev. Appl. **7**, 064023 (2017).

[43] Y.-J. Chen, H. K. Lee, R. Verba, J. A. Katine, I. Barsukov, V. Tiberkevich, J. Q. Xiao, A. N. Slavin, and I. N. Krivorotov, Parametric resonance of magnetization excited by electric field, Nano Lett. **17**, 572 (2017).

[44] T. Yamamoto, T. Nozaki, H. Imamura, S. Tamaru, K. Yakushiji, H. Kubota, A. Fukushima, and S. Yuasa, Voltage-driven magnetization switching controlled by microwave electric field pumping, Nano Lett. **20**, 6012 (2020).

[45] B. Rana and Y. C. Otani, Towards magnonic devices based on voltage-controlled magnetic anisotropy, Commun. Phys. **2**, 90 (2019).